applied sciences

MDPI

Article

A Study of Variable Cell Spacings to the Heat Transfer Efficiency of Air-Cooling Battery Thermal Management System

Gang Zhao *, Xiaolin Wang * and Michael Negnevitsky

School of Engineering, University of Tasmania, Hobart 7005, Australia; Michael.Negnevitsky@utas.edu.au
* Correspondence: gang.zhao@utas.edu.au (G.Z.); xiaolin.wang@utas.edu.au (X.W.)

Featured Application: The research could be applied in the battery thermal management system of electric vehicles. The novel gradient vertical spacing battery cell arrangement design could deliver better cooling performance with almost no cost increase.

Abstract: The air-cooling battery thermal management system has been widely adopted as the thermal management device for power accumulators on electric vehicles nowadays. To improve the system heat transfer coefficient with the minimum rise in cost, this study modified conventional rectangular cell arrangements for 21,700 cylindrical cell battery packs with two approaches: 1. increase the vertical spacings; 2. convert constant vertical spacings to gradient vertical spacings. The results show that smaller vertical spacings are beneficial to the overall cooling performances of the constant vertical spacings designs at almost all flow rates. The gradient vertical spacing design with larger spacing could deliver better temperature uniformity, while the one with smaller spacings could suppress the maximum temperature more efficiently at higher flow rates. However, the total battery pack volume of Design 7 (the largest gradient vertical spacing design) is 7.5% larger than the conventional design.

Keywords: lithium-ion battery; air cooling; battery thermal management system; battery cell spacing; gradient vertical spacing

Citation: Zhao, G.; Wang, X.; Negnevitsky, M. A Study of Variable Cell Spacings to the Heat Transfer Efficiency of Air-Cooling Battery Thermal Management System. *Appl. Sci.* **2021**, *11*, 11155. https://doi.org/10.3390/app112311155

Academic Editor: Dong-Won Kim

Received: 31 October 2021
Accepted: 22 November 2021
Published: 24 November 2021

1. Introduction

Lithium-ion batteries (LIB) have been widely adopted as the onboard power battery cell type for commercial electric vehicles (EV) [1,2]. To provide an ideal operating environment, the battery thermal management system (BTMS) is essential to maintain the battery cell temperatures within a certain range. Air cooling and liquid cooling are two dominant technical routes for commercial EV BTMS. Presumably, the two methods have pros and cons in different aspects. Liquid-cooling BTMS has higher cooling efficiency and capacity at the cost of its high expense and complex structure. Air-cooling BTMS is well-known for its simple structure, robust performance, and safe character (no leakage risk) but delivers a much less efficient cooling performance than its liquid-cooling counterpart [3]. With the fierce competition of commercial EV manufacturing around the world, the overall cost has been more and more underscored by many original equipment manufacturers (OEMs), not only for survival but also for more profits. The strong urge for cost reduction has aroused interest in the air-cooling BTMS. To cope with this economical and technical impulse, this study aims to improve the heat transfer efficiency and cooling performance of a basic air-cooling BTMS design. As can be seen in the relevant review articles, there are many approaches to improve the cooling efficiency of air-cooling BTMSs [4]. Changing the cooling channels, modifying the inlet and outlet, adopting more thermally conductive materials, adding fins and vortex generators, and cell-cooling methods are all effective to improve overall cooling performances. For the cooling channel improvement, one novel approach is to adjust the LIB cell spacings to form variable cooling channels, obtaining different cooling performances.

Many types of research are about optimizing the battery pack cell spacings for either prismatic or cylindrical cells. For prismatic cell battery packs, Fan et al. [5] found smaller gap spacing between cells could lower the temperature rise. Moderate gap spacing was beneficial to improve the temperature uniformity. Uneven gap spacing could improve the temperature distribution but hardly reduce the maximum temperature rise. Zhang et al. [6] proposed a wedge-shaped layout air-cooling BTMS in a row of 12 parallel prismatic cells. The cell clearance was found to affect the flow rate remarkably and cause a higher level of noise. The simulation results also show that smaller clearance (3 mm clearance design is better than both 5 mm and 7 mm clearance designs) was better for heat dissipation at the cost of greater energy consumption. Chen et al. [7] optimized the battery cell spacings of a parallel rectangular battery pack of 12 × 2 prismatic cells. They found the spacing around the hottest cell should be increased while the spacing around the coolest cell should be reduced to obtain a lower maximum temperature and smaller temperature differences. The results show that the adjusted cell spacings remarkably reduced the maximum temperature difference by 42%. Chen et al. [8] investigated the influences of cell number and spacing distribution on the cooling performance of a typical parallel air-cooling BTMS with a rectangular battery pack of N × M prismatic cells. They adjusted the cell spacings to acquire more homogeneous air flow rates within the cooling channels by using the optimization strategy of reducing the gap spacing of the high air flow rate cooling channel and increasing the gap spacing of the low air flow rate cooling channel. The air flow rates within two channels adjacent to the inlet and outlet are suggested to be 70% of the other channels. The maximum temperature and temperature difference were reduced by 4.0 K and 69% by using the cell spacing optimization approach. They also investigated the cooling performance of a symmetrical air-cooling BTMS with an uneven cell-spacing structure [9]. Compared with the asymmetrical system, the maximum temperature and energy consumption of the optimized symmetrical design were decreased by 43% and 33%, respectively.

For cylindrical cell battery packs, Zhao et al. [10] adopted 18,650, 26,650, and 42,110 cylindrical cells in the rectangular designs with three types of inlet and outlet positions to compare the cooling performances. The cell gap spacing size was found not to be too small or too large. The optimal ratio between spacing distance and the cell diameter decreases with the increase of cell diameter. Yang et al. [11] compared the thermal performances of aligned and staggered layouts of 10 × 6 cylindrical cells under a consistent air flow direction. For the same air flow rate, the cooling efficiency is proportional to the longitudinal interval for the aligned arrangement and inversely proportional to the longitudinal interval for the staggered arrangement. The temperature rise is proportional to the transverse interval for both aligned and staggered arrangements.

Generally, there are three types of LIB cells: prismatic cell, pouch cell, and cylindrical cell. Since the pouch and prismatic cells have similar shapes and sizes (usually rectangular flat boards), the BTMS designs for prismatic cell packs are presumably also applicable for the pouch ones. Comparing the quantity of relevant heat transfer research in recent years, there is an observable difference between the quantity of papers on different subjects, with more research conducted on prismatic cells than cylindrical cells. Moreover, the commercial applications of air-cooling BTMS for prismatic or pouch cells (such as Nissan, BYD, and Toyota, etc.) are more common than those for the cylindrical ones (Tesla Motors, Inc. is the most dominant OEM user of cylindrical cells and only uses liquid-cooling BTMS for their thermal management). So, the commercial application of air-cooling BTMS for the cylindrical cell battery pack is another gap that needs more energy and commitments to cross over. The successful commercialization of air-cooling BTMS for cylindrical cells will be a breakthrough for the thermal management of EV cylindrical LIB cells. To fill these gaps, this study focuses on the effects of the cell spacing optimization on the cooling performances of air-cooling BTMS with 21,700 cylindrical LIB cells, which still lacks research in the literature. The optimization works include finding the optimal vertical spacing value and the most effective gradient vertical spacing design. The theoretically proven optimal

design could be further validated by experiments and explored for potential commercial EV applications.

2. 3D Modelling and Cooling Performance Indicators

2.1. Battery Cell Dimensions and Major Parameters

The 3D modelling software used in this study was ANSYS Fluent 2020 R1. The 21,700 cylindrical LIB cell was the prototype of the 3D battery cell model used in this study. The dimensions and major parameters of the cell are listed in Table 1 [12].

Table 1. Dimensions and parameters of the 21,700 cylindrical Lithium-ion battery cell in this study.

Major Parameters	Values
Cell length (mm)	66
Cell diameter (mm)	21
Anode tab diameter (mm)	21
Anode tab height (mm)	2
Cathode tab diameter (mm)	13
Cathode tab height (mm)	2
Active material density (kg/m^3)	2092
Active material Cp (specific heat) (J/kg-K)	678
Active material thermal conductivity (W/m-K)	18.2
Active material electrical conductivity (Siemens/m)	3.541×10^7
Passive material density (kg/m^3)	8978
Passive material Cp (specific heat) (J/kg-K)	381
Passive material thermal conductivity (W/m-K)	387.6
Passive material electrical conductivity (Siemens/m)	1×10^7

2.2. Air-Cooling BTMS Dimensions and Configurations

To fix the overall heat generations, the total cell number of 45 was selected as a typical example in all designs. The 45 cells could be divided into 9 columns with 5 cells in each column, which could provide enough variation margins for the gradient vertical spacing designs (4×3, 5×3, and 6×3 cell arrangement). The 45-cell pack could also be used as one of the basic unit modules for the commercial EV battery pack. Furthermore, considering the calculation cost and computer load, the 45-cell air-cooling BTMS has a reasonable simulation volume for the average desktop in the labs (it takes about 5 h for a complete simulation at each operating condition). The dimensions of all 7 designs are shown in Figure 1. Seven designs include three similar derivative designs in two groups and two sets of opposite flow direction simulations for Design 4. The three variations in each group are meant to be sufficient to reflect the cooling performances of different vertical spacings and uncover the optimal cell spacing values. The horizontal cell spacings in all 7 designs were 30 mm, which was decided based on previous relevant research [13–15]. Design 1 was the basic rectangular 5×9 battery pack. Both its horizontal and vertical spacings are 30 mm. Based on Design 1, the vertical spacings of every column in Design 2 and 3 were increased to 31.5 mm and 33 mm, respectively, by an increment unit of 1.5 mm, which increased the total cell spacing widths (the sum of four cell centre distances) of Design 2 and 3 to 126 mm and 132 mm, respectively. The reason for choosing 1.5 mm as the increment unit of the vertical spacings was that both 126 mm and 132 mm could be divided roundly by 3 (4-cell column), 4 (5-cell column), and 5 (6-cell column) with at most one decimal for the gradient vertical spacing designs. Due to the symmetrical structure of Design 1, 2, and 3, the inlet and outlet configuration of these three designs is similar to what is shown in Figure 2: 5-cell-side inlet and 5-cell-side outlet. Designs 4–7 were based on the concept of uneven vertical spacings: three 4-cell columns, three 5-cell columns, and three 6-cell columns. Design 4 is unique due to its 4-cell-side inlet and 6-cell-side outlet configuration, as shown in Figure 2. Both Design 4 and 5 have the same vertical spacing: 40 mm for the 4-cell column, 30 mm for 5-cell column, and 24 mm for 6-cell column as shown in Figure 1. Opposite to Design 4, Design 5–7 are all 6-cell-side inlet and 4-cell-side

outlet configurations as shown in Figure 2. Based on Design 5, the vertical spacings for the 4-cell column, 5-cell column, and 6-cell column of Design 6 and 7 are 42 and 44 mm, 31.5 and 33 mm, and 25.2 and 26.4 mm, respectively, as shown in Figure 1. According to the vertical spacing patterns of each design, Design 1–3 were collated as the Constant Vertical Spacing Group (CVSG) while Design 4–7 were collated as the Gradient Vertical Spacing Group (GVSG). Design 4 is unique in the GVSG since its inlet/outlet positions are opposite to the other three designs in the group.

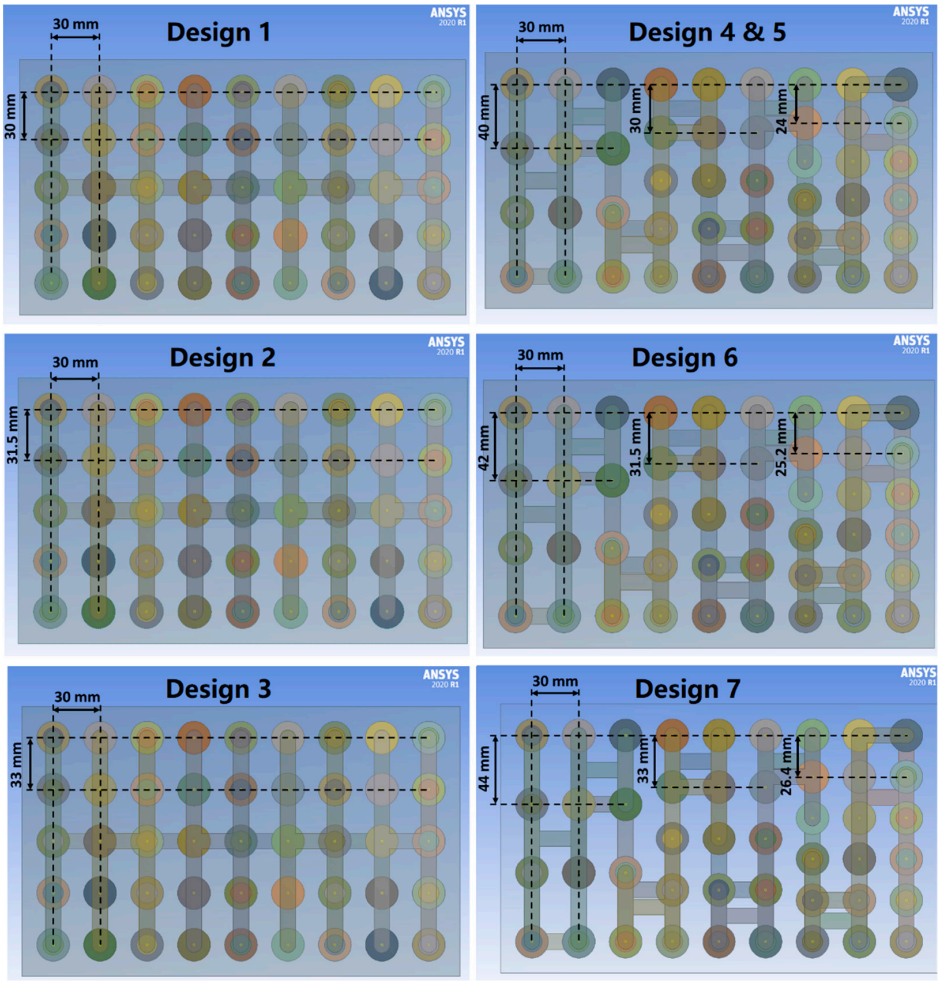

Figure 1. Dimensions of 7 designs.

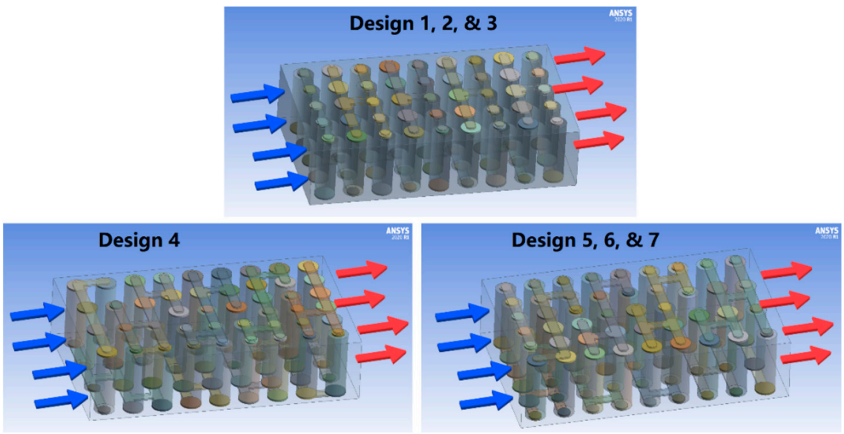

Figure 2. Inlet and outlet configurations of 7 designs.

2.3. Cooling Performance Indicators and Evaluation Criteria

In this study, the maximum temperature (T_{max}), minimum temperature (T_{min}), and maximum temperature difference (ΔT) were used to evaluate the overall cooling performances. The maximum pressure difference (ΔP) was used to indicate the power consumption of the air-cooling BTMS. T_{max} and T_{min} refer to the maximum and minimum temperatures of all cells and busbars surfaces during the discharging process. ΔT is the maximum difference between T_{max} and T_{min} at any time during discharging. According to the general operating characteristics of LIB cells, the battery heat generating rate usually peaks at the end of the discharging, accompanied by the highest cell temperature, so the ΔT values were collected at the last simulation time step. ΔP is the difference between the average pressures of the inlet and outlet. Since ΔP is generally a constant value during the discharging only dependent on the inlet velocity and cooling channel structures, the ΔP values were also collected at the last simulation time step. Theoretically, the desired LIB cell operating temperature range would be from 25 °C to 40 °C [16–21]. The thermal hazards (such as ignition, internal short circuit, combustion, explosion, toxic gases leakage, and thermal runaway, etc.) caused by high temperatures could lead to the early failure of the LIB cells [22–24]. The maximum ΔT is usually set as 5 °C, which is widely elucidated by much relevant research [25–31]. In this study, two major cooling performance evaluation criteria are $T_{max} \leq 35$ °C (308.15 K) and $\Delta T \leq 5$ °C (5 K).

3. Mathematical Models and Validations

In the ANSYS Fluent module, the battery electrochemical model and heat and mass transfer model are two fundamental numerical models used to predict both heat generations during discharging and heat transfer between coolant (air) and cells.

3.1. Battery Electrochemical Model

The dual-potential, multi-scale, multi-domain (MSMD) and electric circuit model (ECM) were selected as the simulation methodologies in this study. The conventional Newman's electrochemistry model is simplified in Equation (1) [32]:

$$\int_V \nabla \cdot (\sigma \nabla \varnothing) dV = \int_A j dA \tag{1}$$

where ∇ is the Del operator, ϕ is the electric potential, j is the volumetric transfer current density, A is the surface area of the interface, and σ is the electrical conductivity.

For the MSMD model, the battery electrical and thermal fields are expressed by Equations (2)–(4) [33]:

$$\frac{\partial \rho_b C p_b T}{\partial t} - \nabla \cdot (k_b \nabla T) = \dot{q} \tag{2}$$

$$\nabla \cdot (\sigma_+ \nabla \varphi_+) = -j \tag{3}$$

$$\nabla \cdot (\sigma_- \nabla \varphi_-) = j \tag{4}$$

where ρ_b is the battery mass density, Cp_b is the battery specific heat capacity, T is the temperature, k_b is the battery thermal conductivity, $\dot{q}$ is the heat generation rate which consists of the Joule heat, the electrochemical reaction heat, and the entropic heat, σ_+ and σ_- are the anode and cathode effective electrical conductivities, and φ_+ and φ_- are the anode and cathode phase potentials.

For the ECM model, a diagram from the work of Chen et al. [34] was proposed to illustrate its mechanism, as shown in Figure 3. It is a surrogate model with six parameters, including 3 resistors and 2 capacitors, to simulate the internal electrochemical behaviours of a LIB cell.

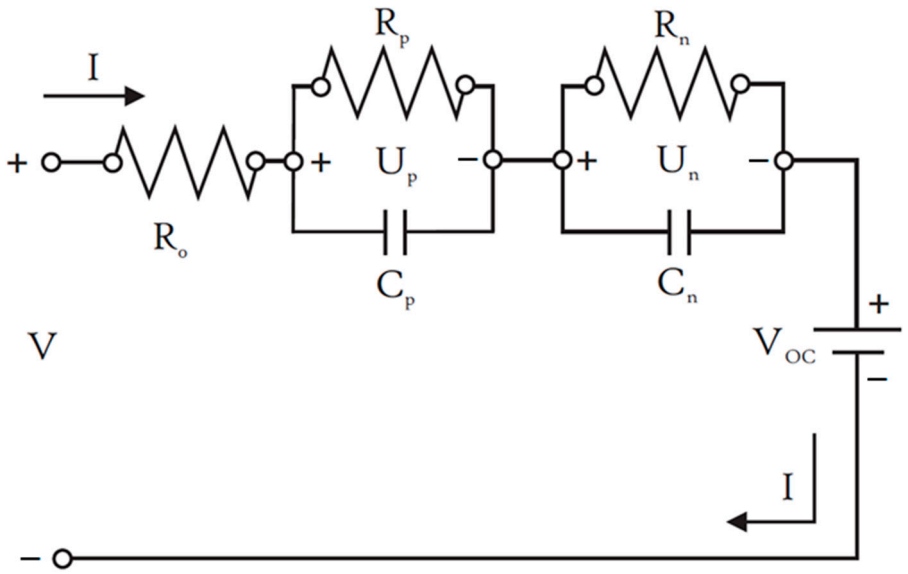

Figure 3. Electric circuit model diagram.

The voltages and currents in the ECM can be solved by Equations (5)–(8) [34]:

$$V(t) = V_{OC}(SoC) + V_p + V_n - R_o(SoC)I(t) \tag{5}$$

$$\frac{dU_p}{dt} = -\frac{1}{R_p(SoC)C_p(SoC)}V_p - \frac{1}{C_p(SoC)}I(t) \tag{6}$$

$$\frac{dU_n}{dt} = -\frac{1}{R_n(SoC)C_n(SoC)}V_n - \frac{1}{C_n(SoC)}I(t) \tag{7}$$

$$\frac{d(SoC)}{dt} = \frac{I(t)}{3600Q_b} \tag{8}$$

where V is the battery voltage, I is the battery current, V_{OC} is the open-circuit voltage, SoC is the state of charge, V_p and V_n are the voltages of R_p/C_p and R_n/C_n, R_o, R_p and R_n are the resistance of resistor o, p, and n, C_p and C_n are the capacitance of capacitor p and n, Q_b is the total battery capacity.

3.2. Mass and Heat Transfer Model

Mass, momentum, and energy conservation equations are three fundamental equations for the mass and heat transfer simulation in ANSYS. For an incompressible ideal gas, the mass conservation is expressed by Equation (9) [35]:

$$\frac{\partial \rho_a}{\partial t} = -\nabla \cdot \left(\rho_a \vec{v}\right) \tag{9}$$

where ρ_a is the air mass density, $\vec{v}$ is the airflow velocity vector.

In an inertial reference frame, the momentum conservation is expressed by Equation (10) [36]:

$$\frac{\partial\left(\rho \vec{v}\right)}{\partial \mathrm{t}} + \nabla \cdot \left(\rho \vec{v}\,\vec{v}\right)) = -\nabla \mathrm{p} + \nabla \cdot (\overline{\overline{\tau}}) \tag{10}$$

where p is the static pressure, $\overline{\overline{\tau}}$ is the stress tensor.

The energy conservation is expressed in Equation (11) [37]:

$$\rho_a C p_a \nabla T_a + \rho_b C p_b \frac{\partial T_b}{\partial \mathrm{t}} = k_a \nabla^2 \mathrm{T}_a + k_b \nabla^2 \mathrm{T}_b + q_b \tag{11}$$

where ρ_a, ρ_b, Cp_a, Cp_b, k_a, k_b, T_a, and T_b are the density, specific heat capacity, thermal conductivity, and temperature of the air and battery, respectively. ∇^2 is the Laplace operator, q_b is the battery heat generation rate.

3.3. Model Validation

The ANSYS Fluent MSMD module could automatically identify the quantities of series or parallel connections from the 3D model of the BTMS based on the correct busbars and cells configurations. The air was set as an incompressible ideal gas with a viscosity of temperature-dependent function following Sutherland's Law. The ECM settings are listed in Table 2.

Table 2. Electric circuit model Settings.

Battery ECM Parameters	Values
Nominal Cell Capacity (Ah)	4
Specified C-Rate	2
Max Stop Voltage (V)	4.3
Min Stop Voltage (V)	2.5
Initial SoC	1
Reference Capacity (Ah)	20

The experimental data from a published paper by Fan et al. [38] were adopted to verify the heat generation and transfer models in this study. Figure 4a shows the validation model of the experimental test rig of 32 pieces (4 × 8) with 18,650 cylindrical cells in an acrylic wind tunnel. The cells are connected in 4p8s connection: every 4 cells in one column are connected in parallel and all 8 columns are connected in series. The experiments were conducted at flow rates of 0.6–4 m/s. Figure 4b shows the CFD mesh effect of the validation model. The horizontal and vertical cell centre distances are both 22 mm. The distance between the cell centre and the acrylic wall is 13 mm. The inlet air temperature and the ambient temperature were 20 °C. The three discharging rates were 0.5, 1C, and 2C.

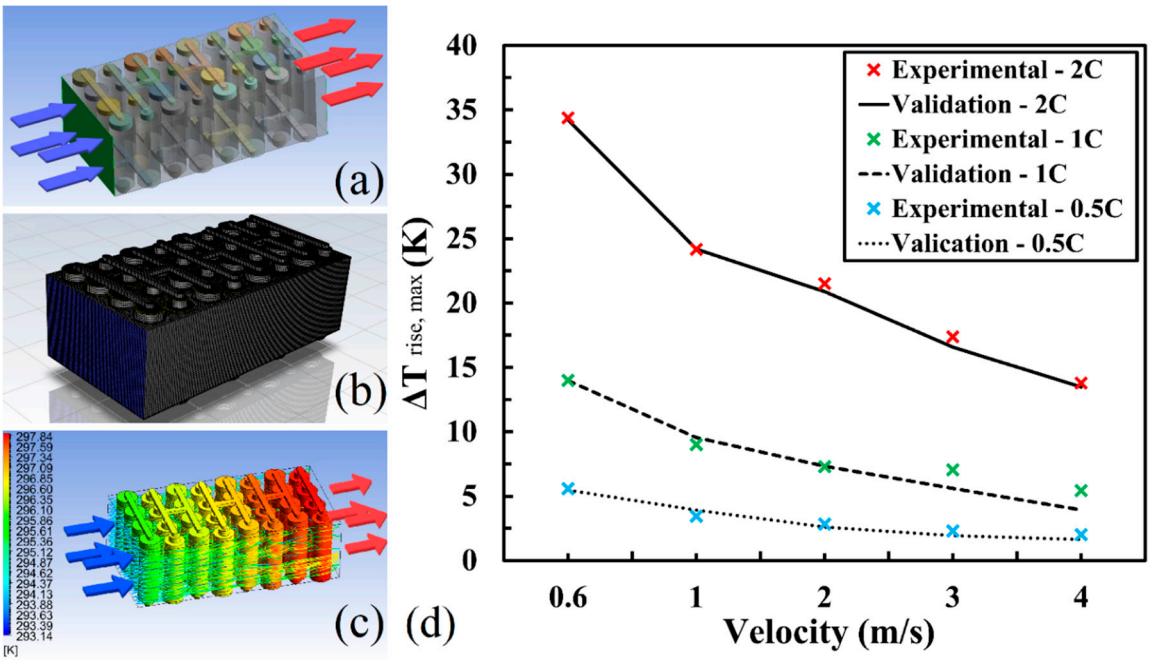

Figure 4. Model validation: (**a**) validation model; (**b**) CFD mesh; (**c**) battery surface temperature contour and air velocity streamlines at 4 m/s 20 °C inlet air during 0.5C discharging; (**d**) the comparison between the experimental data in Ref. [38] and the validation results in this study at 3 different discharging rates.

Figure 4c shows the battery surface temperature contour and air velocity streamlines at 4 m/s 20 °C inlet air during 0.5C discharging. Figure 4d compares the reference experimental results and the simulation results during 0.5C, 1C, and 2C discharging. The average errors of all five velocity scenarios during 0.5C, 1C, and 2C discharging are 0.12 K, 0.47 K, and 0.37 K, respectively. The standard deviations are 0.35 K, 0.94 K, and 0.33 K, respectively. As a result, the comparison successfully demonstrated the accuracy and reliability of the theoretical model to predict both heat generation and transfer of the thermal performances of an air-cooling BTMS in this study.

4. Results and Analysis

As mentioned in Section 2.3, four major indicators (T_{max}, T_{min}, ΔT, and ΔP) were used to evaluate the cooling performance of the air-cooling BTMS designs in this study. Seven designs, as shown in Figure 1, were simulated at 5 different inlet air velocities during 2C discharging. The simulation results are listed in Appendix A Table A1.

4.1. Inlet Air Velocities and Flow Rates

The air flow rate is one of the most crucial parameters of an air-cooling BTMS. It reflects the cooling capacity and the energy consumption of the cooling system. A higher air flow rate delivers higher cooling capacity but unavoidably consumes more parasitic energy from the same battery pack which it cools. The frictional force to the air flow due to cell arrangement and internal structure could cause viscous losses and reduce the pressure and velocity. To have a fair comparison, the inlet air flow rate should be the same for each design to provide an identical initial cooling capacity. Since the inlet sizes of different designs are slightly different due to various vertical spacings, the inlet velocities for each design were, adjusted correspondingly to deliver the same flow rate (10.56×10^{-3} m^3/s) as shown in Table 3.

Table 3. Different inlet and outlet dimensions and inlet velocities to deliver the same flow rate (10.56×10^{-3} m^3/s).

Design	Inlet/Outlet Dimension (m)	Inlet/Outlet Area (m^2)	Battery Pack Volume (m^3)	Inlet Velocity (m/s)	Flow Rate (m^3/s)
1	0.160×0.066	0.010560	2.9568×10^{-3}	1	
2	0.166×0.066	0.010956	3.0677×10^{-3}	0.9639	
3	0.172×0.066	0.011352	3.1786×10^{-3}	0.9302	
4	0.160×0.066	0.010560	2.9568×10^{-3}	1	10.56
5	0.160×0.066	0.010560	2.9568×10^{-3}	1	
6	0.166×0.066	0.010956	3.0677×10^{-3}	0.9639	
7	0.172×0.066	0.011352	3.1786×10^{-3}	0.9302	

Design 1, 4, and 5 have the smallest inlet and outlet size, so their inlet velocity is the highest. On the other hand, Design 3 and 7 have the largest inlet and outlet size, so their inlet velocity is the lowest. Different flow rates require corresponding inlet velocities for different designs, as shown in Table 4. In this study, the five input air flow rates were 10.56×10^{-3} m^3/s, 21.12×10^{-3} m^3/s, 31.68×10^{-3} m^3/s, 42.24×10^{-3} m^3/s, and 52.8×10^{-3} m^3/s.

Table 4. Different inlet velocities for each design to deliver five input flow rates.

Inlet Velocities (m/s)	Flow Rate (10.56×10^{-3} m^3/s)	Flow Rate (21.12×10^{-3} m^3/s)	Flow Rate (31.68×10^{-3} m^3/s)	Flow Rate (42.24×10^{-3} m^3/s)	Flow Rate (52.80×10^{-3} m^3/s)
Design 1	1.0000 m/s	2.0000 m/s	3.0000 m/s	4.0000 m/s	5.0000 m/s
Design 2	0.9639 m/s	1.9278 m/s	2.8917 m/s	3.8556 m/s	4.8195 m/s
Design 3	0.9302 m/s	1.8604 m/s	2.7906 m/s	3.7208 m/s	4.6510 m/s
Design 4	1.0000 m/s	2.0000 m/s	3.0000 m/s	4.0000 m/s	5.0000 m/s
Design 5	1.0000 m/s	2.0000 m/s	3.0000 m/s	4.0000 m/s	5.0000 m/s
Design 6	0.9639 m/s	1.9278 m/s	2.8917 m/s	3.8556 m/s	4.8195 m/s
Design 7	0.9302 m/s	1.8604 m/s	2.7906 m/s	3.7208 m/s	4.6510 m/s

4.2. Maximum Temperature

Among the four indicators, T_{max} is generally regarded as the most crucial one since it directly shows the cooling capacity of the BTMS. The T_{max} of seven designs at five flow rates are shown in Figure 5. Design 4 always exhibited the highest T_{max} at the five flow rates. The gradient vertical spacing design with a four-cell-side inlet and six-cell-side outlet had the lowest cooling efficiency in terms of the temperature rise among all designs. Design 1 had the lowest T_{max} (315.91 K and 308.78 K) at 10.56×10^{-3} m^3/s and 21.12×10^{-3} m^3/s, respectively, indicating the smallest cell spacing with a regular 5×9 arrangement could most effectively suppress the temperature rise at lower air flow rates, as shown in Figure 6. At 10.56×10^{-3} m^3/s flow rate, all three designs in the CVSG showed better cooling performances than the three designs (six-cell-side inlet) in the GVSG. When the flow rate rose to 21.12×10^{-3} m^3/s, Design 5 and 6 showed lower T_{max} (309.32 K and 309.67 K) than Design 2 and 3 (310.19 K and 310.24 K), but still higher than Design 1 (308.78 K). At all five flow rates, the T_{max} of Design 3 (317.05 K, 310.24 K, 307.19 K, 305.04 K, and 303.53 K) were always larger than Design 2 (316.52 K, 310.19 K, 306.98 K, 304.82 K, and 303.33 K), indicating the ineffectiveness of increasing vertical spacing values for the constant vertical spacing designs.

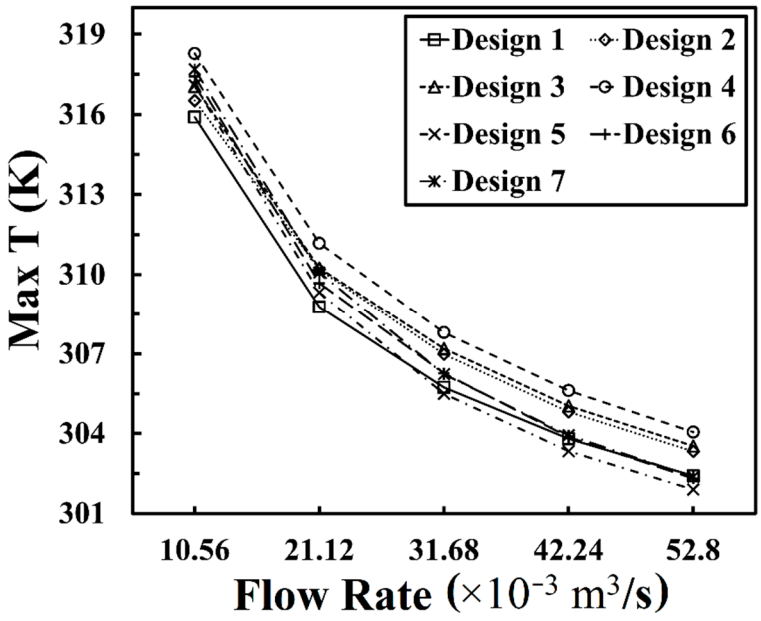

Figure 5. Maximum temperatures of 7 designs at 5 flow rates.

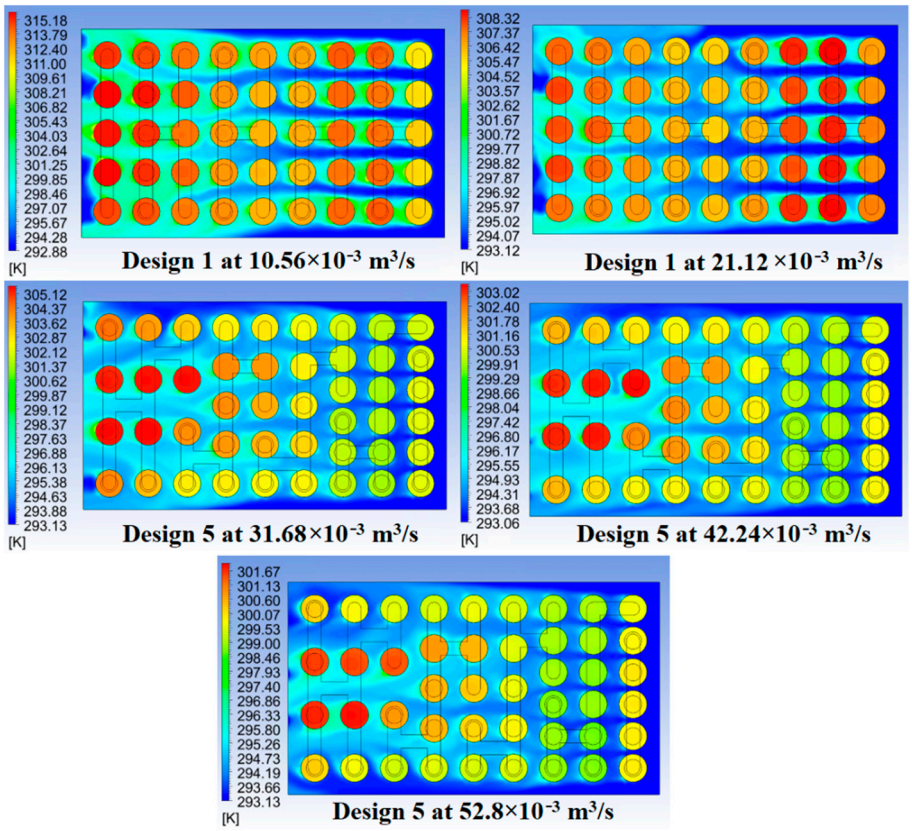

Figure 6. Optimal design (lowest T_{max}) at each flow rate.

The turning point of better cooling performance of gradually emerged with the rise of the air flow rates. At 31.68 × 10^{-3} m^3/s, the T_{max} of Design 5 (305.49 K) firstly became the lowest among all designs, as shown in Figure 6. When the flow rate reached the highest value (52.8 × 10^{-3} m^3/s), the T_{max} of Design 5–7 in GVSG (301.90 K, 302.30 K, and 302.28 K) were all lower than that of Design 1 (302.40 K), which was always the lowest in CVSG. With the flow rates increased to 42.24 × 10^{-3} m^3/s and 52.8 × 10^{-3} m^3/s, Design 5 continued to output the lowest T_{max} values (303.33 K and 301.90 K), as shown in Figure 6. Moreover, just like the pattern in CVSG that Design 1 (30 mm spacing) delivered the lowest T_{max} among three designs (30 mm, 31.5 mm, and 33 mm spacing) at all five flow rates, the T_{max} of Design 5 (40/30/24 mm spacing) was always the lowest among three designs (40/30/24 mm, 42/31.5/25.2 mm, and 44/33/26.4 mm spacing) in GVSG at all five flow rates. Increasing the gradient vertical spacing values was proven to be useless in reducing the T_{max} of constant or gradient vertical spacing designs.

4.3. Minimum Temperature

Since T_{min} is not the direct evaluation criterion, it is not as important as other indicators such as T_{max} and ΔT. The T_{min} of seven designs at five flow rates are shown in Figure 7. Design 5 consistently showed the lowest T_{min} (307.55 K, 303.74 K, 301.14 K, 299.60 K, and 298.55 K) at all five flow rates, towering above the other designs in terms of the temperature reduction capacity. The deduction of T_{max} and T_{min}, i.e., ΔT, is a direct evaluation criterion which should be lower than 5 K. Therefore, higher T_{min} is better since lower T_{min} could result in higher ΔT adversely, triggering the violation of the evaluation criterion of ΔT ($\leq$5 K). Design 2 and Design 3 were both proven to deliver higher T_{min} values at five flow rates, showing the temperature reduction incapacity of the CVSG designs with larger vertical spacings (31.5 mm and 33 mm). On the other hand, the GVSG designs with smaller spacings (40/30/24 mm and 42/31.5/25.2 mm) delivered lower T_{min} values at five

flow rates, which could also insinuate the poor temperature uniformity performances of Design 5 and 6.

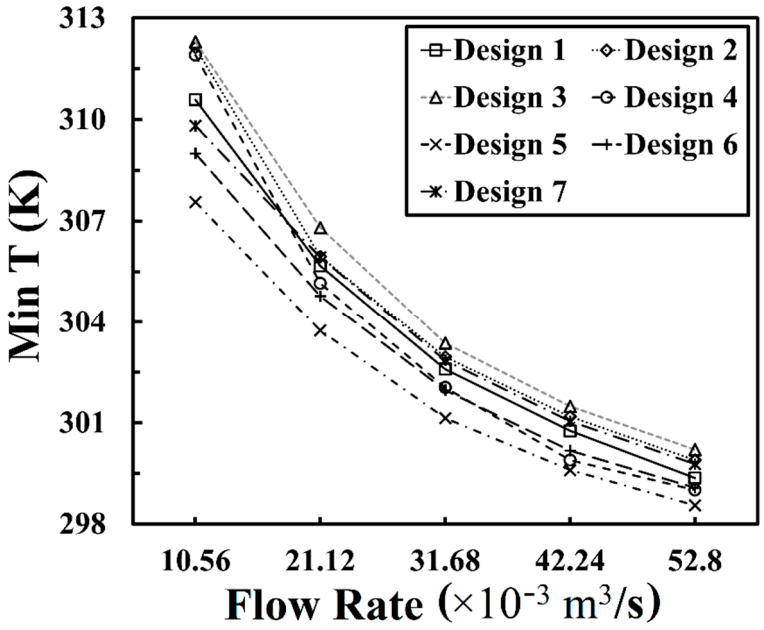

Figure 7. Minimum temperatures of 7 designs at 5 flow rates.

4.4. Temperature Difference

As another direct evaluation criterion, ΔT reflects the temperature uniformity of a BTMS. Figure 8 shows the ΔT of seven designs at five flow rates. At 10.56×10^{-3} m^3/s, only Design 2 (4.40 K) and Design 3 (4.75 K) met the evaluation criterion of ΔT (≤5 K). The GVSG designs (Design 5–7) showed an average ΔT of 8.61 K, revealing the poor temperature uniformity of the gradient vertical spacing designs at low flow rates. Figure 9 shows the air flow velocity streamlines and temperature contour of Design 6 at 10.56×10^{-3} m^3/s. The locations with red (higher) velocity streamlines (especially at the vertical clearances of the six-cell columns close to the inlet) are usually the places where sufficient heat transfer between air flow and battery cells is conducted, leading to lower cell temperatures. On the contrary, the air flow velocity streamlines along the wider vertical cell clearances in the four-cell columns close to the outlet are much lower (the green velocity streamline represents nearly half of the velocity of the red one), leading to less heat transfer and the higher temperature distributions of the surrounding cells.

When the flow rates reached 21.12×10^{-3} m^3/s, the ΔT values of Design 1–3 (3.11 K, 4.24 K, and 3.83 K) were all lower than 5 K and lower than those of Design 5–7 (5.58 K, 4.90 K, and 4.15 K). At 31.68×10^{-3} m^3/s, all designs except Design 4 delivered ΔT lower than 5 K. The average ΔT of CVSG (3.67 K) was 0.34 K lower than that of GVSG (4.01 K). The turning point appeared when the flow rate reached 42.24×10^{-3} m^3/s, Design 7 started to deliver the lowest ΔT (2.88 K) among all designs. Design 1 dropped to second place in terms of the temperature uniformity performance and its advantages over Design 2, 3, 5, and 6 gradually shrank with the increase of the flow rates. At 52.8×10^{-3} m^3/s, the leading margin of ΔT of Design 7 (2.6 K) increased to 0.44 K over Design 1 (3.04 K). At higher air flow rates, the temperature uniformity of the gradient vertical spacing designs with larger spacing values (44/33/26.4 mm) improves more than that of the constant vertical spacing designs.

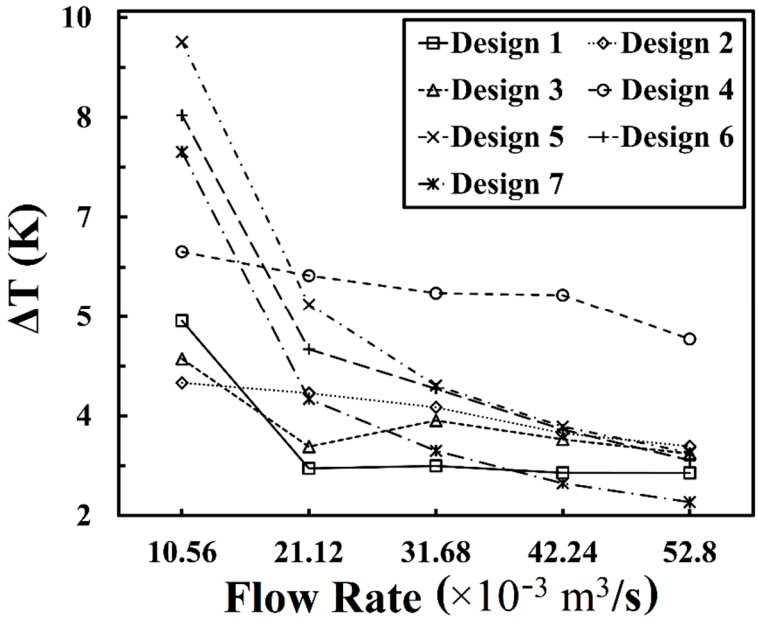

Figure 8. Temperature differences of 7 designs at 5 flow rates.

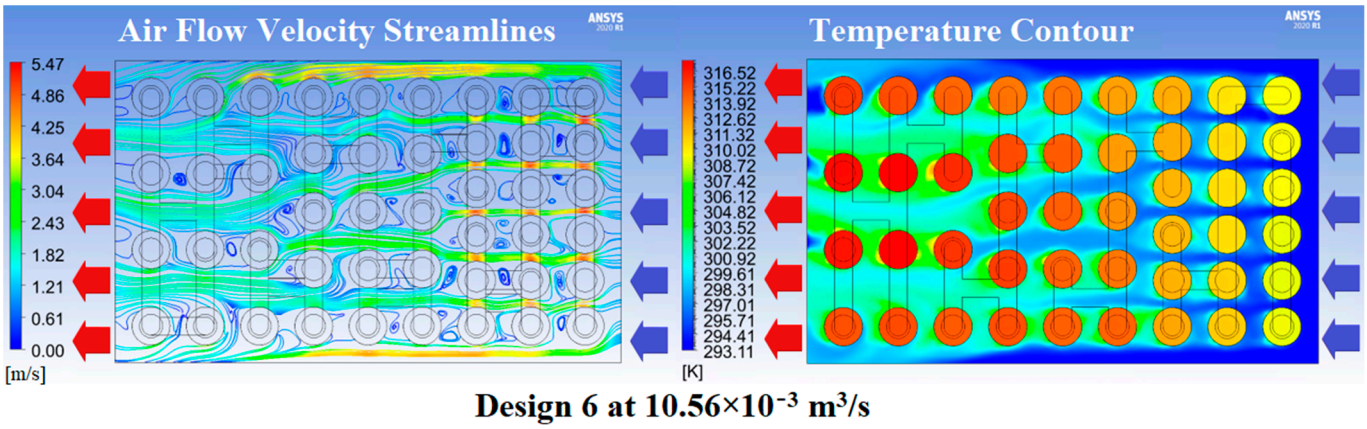

Figure 9. Air flow velocity streamlines and temperature contour of Design 6 at 10.56 × 10^{-3} m^3/s.

4.5. Pressure Difference

As an indirect indicator of the thermal performance, ΔP reflects the overall energy consumption of the air-cooling BTMS. Since two evaluation criteria (T_{max} and ΔT) should be regarded as priorities, ΔP is regarded as a secondary indicator to evaluate and compare the designs when their cooling performances (T_{max} and ΔT) are close. In the EV accumulator system, the energy used to cool the battery pack is the parasitic energy from the battery pack itself, so the lower energy consumption (lower ΔP) of the BTMS could save more energy to extend driving mileage or for other EV functions, such as electronic control systems, lights, heating, ventilation, and air conditioning, etc. The ΔP values of seven designs at five flow rates are shown in Figure 10.

As mentioned in Section 2.3, ΔP is only dependent on the inlet velocity and the intrinsic internal structure of the system. Its values have a constantly rising trend with the increase of the flow rates for each design and the rankings of the ΔP values of each design remained unchanged at all flow rates (from high to low): Design 4, Design 5, Design 6, Design 1, Design 7, Design 2, and Design 3. Design 4 can be considered as the worst design in this study due to having the worst cooling performance and highest energy consumption. Design 3 has the lowest ΔP values at five flow rates due to its constant vertical spacing arrangement and largest cell spacing. Although Design 7 has a gradient vertical spacing

arrangement, it has the second lowest ΔP due to having the largest cell spacing among the GVSG (the inlet areas of Design 7 and Design 3 are the same). A similar trend can be found in Design 2 and Design 6. The constant vertical spacing designs have lower ΔP values than the gradient vertical spacing ones when the total cell spacings (inlet/outlet sizes) are the same.

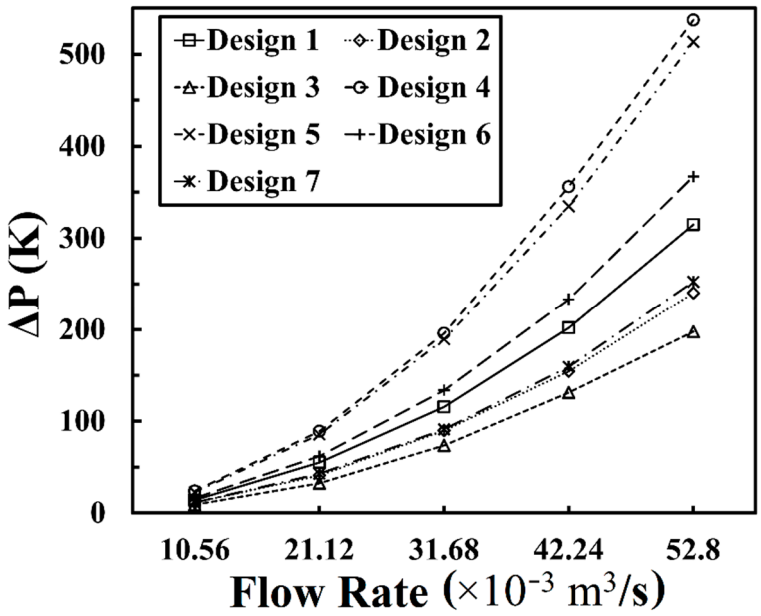

Figure 10. Pressure differences of 7 designs at 5 flow rates.

5. Discussion

In this study, meeting two evaluation criteria was the premise of a qualified air-cooling BTMS design. The evaluation criterion of T_{max} (<308.15 K) could be achieved by all designs when the flow rate reached 31.68 × 10^{-3} m^3/s. Design 5 delivered the lowest T_{max} of 305.49 K, 303.33 K, and 301.90 K at the flow rates of 31.68 × 10^{-3} m^3/s, 42.24 × 10^{-3} m^3/s, and 52.8 × 10^{-3} m^3/s, respectively. The evaluation criterion of ΔT (<5 K) could be achieved by Design 2 and 3 at 10.56 × 10^{-3} m^3/s, Design 1, 2, 3, 6, and 7 at 21.12 × 10^{-3} m^3/s, as well as Design 1, 2, 3, 5, 6, and 7 at 31.68 × 10^{-3} m^3/s, 42.24 × 10^{-3} m^3/s, and 52.8 × 10^{-3} m^3/s, respectively. To make a comprehensive yet balanced comparison, Table 5 lists the performance rankings and status of the two evaluation criteria indicators (T_{max} and ΔT) of each design at five flow rates. The green cell shading means the design inside met the evaluation criteria (T_{max} < 308.15 K or ΔT < 5 K).

Table 5. A ranking and status of each design for two evaluation criteria.

	Flow Rate (×10^{-3} m^3/s)	Design 1	Design 2	Design 3	Design 4	Design 5	Design 6	Design 7
T_{max} (<308.15 K)	10.56	1 [a]	2	3	7	4	5	6
	21.12	1	5	6	7	2	3	4
	31.68	2 [b]	5	6	7	1	4	3
	42.24	2	5	6	7	1	3	4
	52.80	4	5	6	7	1	2	3
ΔT (<5 K)	10.56	3	1	2	4	7	6	5
	21.12	1	4	2	7	6	5	3
	31.68	1	4	3	7	6	5	2
	42.24	2	4	3	7	6	5	1
	52.80	2	6	4	7	5	3	1

[a] Grey cell shading—did not meet the evaluation criterion. [b] No cell shading—met the evaluation criterion.

When the flow rates were 10.56×10^{-3} m^3/s and 21.12×10^{-3} m^3/s, none of the designs could meet the requirement of T_{max}, and only half of the designs could meet the requirement of ΔT. At 10.56×10^{-3} m^3/s, Design 2 is considered as the optimal design due to coming in first place in ΔT (4.4 K) and second place in T_{max} (316.52 K), though it is unqualified.

At 21.12×10^{-3} m^3/s, Design 1 is the optimal one due to its leading positions in both T_{max} (308.78 K) and ΔT (3.11 K), though it is also unqualified. Design 3 ranks second in ΔT (3.44 K) and Design 5 ranks second in T_{max} (309.32 K), but their other indicators (T_{max} of Design 3 and ΔT of Design 5) are both coincidently ranked sixth.

At 31.68×10^{-3} m^3/s, Design 1 firstly met both evaluation criteria and continued to hold its top position for its first place in ΔT (3.14 K) and second in T_{max} (305.74 K). Although Design 5 delivers the lowest T_{max} (305.49 K), its ΔT (4.35 K) is 0.24 K higher than the average ΔT of all designs (4.11 K).

At 42.24×10^{-3} m^3/s, T_{max} of Design 5 (303.33 K) was 0.47 K lower than Design 1 (303.80 K), but the ΔT of Design 5 (3.74 K) was 0.7 K higher than Design 1 (3.04 K). Meanwhile, ΔT of Design 7 (2.88 K) was 0.16 K and 0.86 K lower than Design 1 (3.04 K) and Design 5 (3.74 K), respectively. However, T_{max} of Design 7 (303.93 K) was 0.13 K and 0.6 K higher than Design 1 (303.8 K) and Design 5 (303.33 K). Therefore, the optimal design at 42.24×10^{-3} m^3/s becomes a conditional evaluation depending on the aspect in priority: 1. Design 5 is optimal if lower T_{max} is the major objective; 2. Design 7 is optimal if ΔT is mostly concerned; 3. Design 1 is optimal if a balanced thermal performance is required.

At 52.8×10^{-3} m^3/s, the T_{max} of Design 1 (302.4 K), Design 2 (303.33 K), and Design 3 (303.53 K) in CVSG rank fourth, fifth, and sixth, respectively. On the contrary, the T_{max} of Design 5 (301.9 K), Design 6 (302.3 K), and Design 7 (302.38 K) in GVSG rank first, second, and third, respectively, demonstrating a significant cooling advantage of the gradient vertical spacing designs over the constant vertical spacing ones at higher flow rates. For the ΔT, Design 7 (2.6 K) is 0.44 K lower than Design 1 (3.04 K) while Design 2 (3.44 K), Design 3 (3.33 K), Design 5 (3.34 K), and Design 6 (3.23 K) are very close to each other. As a result, Design 7 is the optimal design at 52.8×10^{-3} m^3/s.

As a specific reference and negative case to the GVSG, Design 4 almost came in last place in both evaluation criteria at all flow rates (except the fourth place of ΔT at 10.56×10^{-3} m^3/s). The gradient vertical spacing design with fewer cell side inlets (four-cell-side inlet/six-cell-side outlet) has been proven to be the most ineffective air-cooling BTMS design. As discussed in some previous studies, the reason could be explained by the field synergy principle (FSP); the temperature gradient field vector within the battery pack (from higher temperature side, i.e., six-cell-side, to lower temperature side, i.e., four-cell-side) is 180 degrees opposite to the air velocity field vector (from four-cell-side inlet to six-cell-side outlet), which significantly violates the essence of the FSP; reducing the intersection angle between velocity and temperature gradient field vectors could enhance the heat transfer coefficient. So, for the gradient vertical spacing design, the inlet should always be put on the side with a greater cell quantity.

Generally, 2C discharging is not a small operating current for EVs. Theoretically, the average EV discharging rate should be 0.1C if the fully charged battery pack could provide a 10 h operating length. One finding in this study was that larger vertical spacing for the constant vertical spacing designs was unable to improve the cooling performances of the air-cooling BTMS. On the contrary, it would adversely increase the total volume of the battery pack. For the EV applications, it is important to find the optimal spacing value (reasonably smaller value) which could both deliver top cooling performance and save space. The gradient vertical spacing design could deliver better cooling performance when the inlet air flow rate is high. We recommend that this property is applied to the high power or performance EVs whose short-term discharging rate could reach 5C or higher. However, the compromise is that its low flow rate cooling performance is not as efficient as the constant vertical spacing design. Different spacing designs shall be applied

to their favourable working scenarios according to the specific requirement and operating characteristics of the real EV applications.

As mentioned in Section 2.2, a 45-cell pack is a limited yet reasonable size for a basic unit module in an EV battery pack. The size needs to be larger if the actual battery power or capacity demands of the EV are higher. Larger battery packs will also consume more computational and time resources. So, a larger air-cooling BTMS unit of around 100 cylindrical cells will be a future extension of this study. In addition, the experimental validations will also be carried out in the near future to not only prove this theoretical study, but also brighten our research in this field.

6. Conclusions

This study compared the cooling performances of constant vertical spacing and gradient vertical spacing designs with different vertical spacing values at five flow rates. The simulation results showed that increasing the vertical spacing values of the constant vertical spacing design was ineffective in reducing either T_{max} or ΔT. Smaller spacing (30 mm) was always beneficial, reducing both T_{max} and ΔT of constant spacing designs at different flow rates. The gradient vertical spacing designs had a worse thermal performance at lower flow rates (10.56×10^{-3} m^3/s and 21.12×10^{-3} m^3/s), especially since the temperature uniformity was unsatisfactory. However, with the increase of flow rate (52.8×10^{-3} m^3/s), the gradient vertical spacing design with larger gradient vertical spacings (44/33/26.4 mm) exhibited superb temperature uniformity (ΔT = 2.6 K) while the gradient vertical spacing design with smaller gradient vertical spacings (40/30/24 mm) suppressed the T_{max} under 301.9 K, showing the potential of the gradient vertical spacing designs to enhance the upper limit of the system cooling capacities. For the ΔP, the gradient vertical spacing designs always show higher values than the constant vertical spacing ones when the inlet and outlet sizes are equal. Besides, the larger vertical spacing could adversely increase the total volume of the air-cooling BTMS by 3.75% (Design 2 and 6) and 7.5% (Design 3 and 7) compared to the basic design (Design 1, 4, and 5). A reasonable trade-off between cooling performance, energy consumption, and volume should always be made according to the requirements of the EV battery pack.

Author Contributions: Conceptualization, G.Z., X.W. and M.N.; methodology, G.Z., X.W. and M.N.; supervision, X.W. and M.N.; software, G.Z.; validation, G.Z.; formal analysis, G.Z.; investigation, G.Z., X.W. and M.N.; resources, X.W.; data curation, G.Z.; writing—original draft preparation, G.Z.; writing—review and editing, X.W. and M.N.; project administration, X.W.; funding acquisition, X.W. and M.N. All authors have read and agreed to the published version of the manuscript.

Funding: This research was funded by the Australian Research Council, grant number LP170100879.

Institutional Review Board Statement: Not applicable.

Informed Consent Statement: Not applicable.

Conflicts of Interest: The authors declare no conflict of interest.

Nomenclature

A	battery surface area (m^2)
C	capacitance (F)
Cp	specific heat capacity ($J \cdot kg^{-1} \cdot K^{-1}$)
I	current (A)
j	current density ($A \cdot m^{-2}$)
k	thermal conductivity ($W \cdot m^{-1} \cdot K^{-1}$)
P, p	pressure (Pa)
Q	battery capacity (Ah)
q	heat generation rate ($W \cdot m^{-3}$)
R	resistance (Ω)

T	temperature (°C, K)
V	voltage (V)
v	air flow velocity ($m \cdot s^{-1}$)
Greek symbols	
Δ	difference
ρ	mass density ($kg \cdot m^{-3}$)
σ	electrical conductivity ($Siemens \cdot m^{-1}$)
$\bar{\bar{\tau}}$	viscous stress tensor (Pa)
φ	phase potential (V)
ϕ	electric potential (V)
∇	Gradient operator, represents the partial derivative of a quantity with respect to all directions in the chosen coordinate system (m^{-1})
∇^2	Laplace operator, represents the sum of second partial derivatives of the function with respect to each independent variable in a Cartesian coordinate system (m^{-2})
Subscripts	
+	anode
−	cathode
a	air
b	battery
max	maximum
min	minimum
OC	open circuit
Abbreviations	
BTMS	battery thermal management system
CVSG	constant vertical spacing group
ECM	electric circuit model
EV	electric vehicle
FSP	field synergy principle
GVSG	gradient vertical spacing group
LIB	lithium-ion battery
MSMD	multi scale multi domain
OEM	original equipment manufacturer
SoC	state of charge

Appendix A

Table A1. Simulation results of 7 designs at 5 different inlet air velocities during 2C discharging.

	Inlet Flow Rate ($\times 10^{-3}$ m^3/s)	**Design 1**	**Design 2**	**Design 3**	**Design 4**	**Design 5**	**Design 6**	**Design 7**
T_{max}	10.56	315.91	316.52	317.05	318.28	317.09	317.43	317.69
	21.12	308.78	310.19	310.24	311.18	309.32	309.67	310.08
	31.68	305.74	306.98	307.19	307.80	305.49	306.27	306.23
	42.24	303.80	304.82	305.04	305.62	303.33	303.87	303.93
	52.80	302.40	303.33	303.53	304.06	301.90	302.30	302.38
T_{min}	10.56	310.58	312.12	312.30	311.90	307.55	308.99	309.81
	21.12	305.67	305.95	306.80	305.16	303.74	304.78	305.93
	31.68	302.59	302.95	303.36	302.05	301.14	301.96	302.85
	42.24	300.76	301.18	301.49	299.89	299.60	300.18	301.05
	52.80	299.37	299.89	300.20	299.00	298.55	299.07	299.78
ΔT	10.56	5.33	4.40	4.75	6.38	9.53	8.43	7.88
	21.12	3.11	4.24	3.44	6.02	5.58	4.90	4.15
	31.68	3.14	4.03	3.83	5.76	4.35	4.31	3.37
	42.24	3.04	3.64	3.55	5.72	3.74	3.69	2.88
	52.80	3.04	3.44	3.33	5.05	3.34	3.23	2.60
ΔP	10.56	14.15	11.31	9.05	23.84	22.50	16.06	11.42
	21.12	55.06	40.90	32.26	89.06	85.66	61.82	42.73
	31.68	115.70	89.75	73.55	196.00	189.60	133.59	91.10
	42.24	202.02	154.49	131.26	356.09	334.80	233.41	159.34
	52.80	314.86	240.33	197.78	537.13	513.49	367.07	252.43

References

1. Hou, J.; Yang, Y.; He, H.; Gao, T. Adaptive dual extended Kalman filter based on variational bayesian approximation for joint estimation of lithium-ion battery state of charge and model parameters. *Appl. Sci.* **2019**, *9*, 1726. [CrossRef]
2. Gourley, S.W.D.; Or, T.; Chen, Z. Breaking free from cobalt reliance in lithium-ion batteries. *Iscience* **2020**, *23*, 101505. [CrossRef]
3. Ye, B.; Rubel, M.R.H.; Li, H. Design and optimization of cooling plate for battery module of an electric vehicle. *Appl. Sci.* **2019**, *9*, 754. [CrossRef]
4. Zhao, G.; Wang, X.; Negnevitsky, M.; Zhang, H. A review of air-cooling battery thermal management systems for electric and hybrid electric vehicles. *J. Power Sources* **2021**, *501*, 230001. [CrossRef]
5. Fan, L.; Khodadadi, J.; Pesaran, A.A. A parametric study on thermal management of an air-cooled lithium-ion battery module for plug-in hybrid electric vehicles. *J. Power Sources* **2013**, *238*, 301–312. [CrossRef]
6. Zhang, J.; Kang, H.; Wu, K.; Li, J.; Wang, Y. The impact of enclosure and boundary conditions with a wedge-shaped path and air cooling for battery thermal management in electric vehicles. *Int. J. Energy Res.* **2018**, *42*, 4054–4069. [CrossRef]
7. Chen, K.; Wang, S.; Song, M.; Chen, L. Configuration optimization of battery pack in parallel air-cooled battery thermal management system using an optimization strategy. *Appl. Therm. Eng.* **2017**, *123*, 177–186. [CrossRef]
8. Chen, K.; Song, M.; Wei, W.; Wang, S. Design of the structure of battery pack in parallel air-cooled battery thermal management system for cooling efficiency improvement. *Int. J. Heat Mass Transf.* **2019**, *132*, 309–321. [CrossRef]
9. Chen, K.; Chen, Y.; She, Y.; Song, M.; Wang, S.; Chen, L. Construction of effective symmetrical air-cooled system for battery thermal management. *Appl. Therm. Eng.* **2020**, *166*, 114679. [CrossRef]
10. Zhao, J.; Rao, Z.; Huo, Y.; Liu, X.; Li, Y. Thermal management of cylindrical power battery module for extending the life of new energy electric vehicles. *Appl. Therm. Eng.* **2015**, *85*, 33–43. [CrossRef]
11. Yang, N.; Zhang, X.; Li, G.; Hua, D. Assessment of the forced air-cooling performance for cylindrical lithium-ion battery packs: A comparative analysis between aligned and staggered cell arrangements. *Appl. Therm. Eng.* **2015**, *80*, 55–65. [CrossRef]
12. Waldmann, T.; Scurtu, R.-G.; Richter, K.; Wohlfahrt-Mehrens, M. 18650 vs. 21700 Li-ion cells–A direct comparison of electrochemical, thermal, and geometrical properties. *J. Power Sources* **2020**, *472*, 228614. [CrossRef]
13. Wang, H.; He, F.; Ma, L. Experimental and modeling study of controller-based thermal management of battery modules under dynamic loads. *Int. J. Heat Mass Transf.* **2016**, *103*, 154–164. [CrossRef]
14. Huo, Y.; Rao, Z. The numerical investigation of nanofluid based cylinder battery thermal management using lattice Boltzmann method. *Int. J. Heat Mass Transf.* **2015**, *91*, 374–384. [CrossRef]
15. Zhang, Y.; Song, X.; Ma, C.; Hao, D.; Chen, Y. Effects of the structure arrangement and spacing on the thermal characteristics of Li-ion battery pack at various discharge rates. *Appl. Therm. Eng.* **2020**, *165*, 114610. [CrossRef]
16. Pesaran, A.A. Battery thermal models for hybrid vehicle simulations. *J. Power Sources* **2002**, *110*, 377–382. [CrossRef]
17. Zhao, C.; Cao, W.; Dong, T.; Jiang, F. Thermal behavior study of discharging/charging cylindrical lithium-ion battery module cooled by channeled liquid flow. *Int. J. Heat Mass Transf.* **2018**, *120*, 751–762. [CrossRef]
18. Zhao, C.; Sousa, A.C.; Jiang, F. Minimization of thermal non-uniformity in lithium-ion battery pack cooled by channeled liquid flow. *Int. J. Heat Mass Transf.* **2019**, *129*, 660–670. [CrossRef]
19. Patil, M.S.; Seo, J.-H.; Panchal, S.; Jee, S.-W.; Lee, M.-Y. Investigation on thermal performance of water-cooled Li-ion pouch cell and pack at high discharge rate with U-turn type microchannel cold plate. *Int. J. Heat Mass Transf.* **2020**, *155*, 119728. [CrossRef]
20. Ye, Y.; Shi, Y.; Saw, L.H.; Tay, A.A. Performance assessment and optimization of a heat pipe thermal management system for fast charging lithium ion battery packs. *Int. J. Heat Mass Transf.* **2016**, *92*, 893–903. [CrossRef]
21. Monika, K.; Chakraborty, C.; Roy, S.; Dinda, S.; Singh, S.A.; Datta, S.P. Parametric investigation to optimize the thermal management of pouch type lithium-ion batteries with mini-channel cold plates. *Int. J. Heat Mass Transf.* **2021**, *164*, 120568. [CrossRef]
22. Ouyang, D.; Chen, M.; Huang, Q.; Weng, J.; Wang, Z.; Wang, J. A review on the thermal hazards of the lithium-ion battery and the corresponding countermeasures. *Appl. Sci.* **2019**, *9*, 2483. [CrossRef]
23. Li, W.; Rao, S.; Xiao, Y.; Gao, Z.; Chen, Y.; Wang, H.; Ouyang, M. Fire boundaries of lithium-ion cell eruption gases caused by thermal runaway. *Iscience* **2021**, *24*, 102401. [CrossRef]
24. Xiong, R.; Ma, S.; Li, H.; Sun, F.; Li, J. Toward a safer battery management system: A critical review on diagnosis and prognosis of battery short circuit. *Iscience* **2020**, *23*, 101010. [CrossRef] [PubMed]
25. Lai, Y.; Wu, W.; Chen, K.; Wang, S.; Xin, C. A compact and lightweight liquid-cooled thermal management solution for cylindrical lithium-ion power battery pack. *Int. J. Heat Mass Transf.* **2019**, *144*, 118581. [CrossRef]
26. Sheng, L.; Su, L.; Zhang, H.; Li, K.; Fang, Y.; Ye, W.; Fang, Y. Numerical investigation on a lithium ion battery thermal management utilizing a serpentine-channel liquid cooling plate exchanger. *Int. J. Heat Mass Transf.* **2019**, *141*, 658–668. [CrossRef]
27. Zou, D.; Ma, X.; Liu, X.; Zheng, P.; Hu, Y. Thermal performance enhancement of composite phase change materials (PCM) using graphene and carbon nanotubes as additives for the potential application in lithium-ion power battery. *Int. J. Heat Mass Transf.* **2018**, *120*, 33–41. [CrossRef]
28. Yan, J.; Wang, Q.; Li, K.; Sun, J. Numerical study on the thermal performance of a composite board in battery thermal management system. *Appl. Therm. Eng.* **2016**, *106*, 131–140. [CrossRef]

29. Shang, Z.; Qi, H.; Liu, X.; Ouyang, C.; Wang, Y. Structural optimization of lithium-ion battery for improving thermal performance based on a liquid cooling system. *Int. J. Heat Mass Transf.* **2019**, *130*, 33–41. [CrossRef]
30. Choudhari, V.; Dhoble, A.; Panchal, S. Numerical analysis of different fin structures in phase change material module for battery thermal management system and its optimization. *Int. J. Heat Mass Transf.* **2020**, *163*, 120434. [CrossRef]
31. Pan, M.; Zhong, Y. Experimental and numerical investigation of a thermal management system for a Li-ion battery pack using cutting copper fiber sintered skeleton/paraffin composite phase change materials. *Int. J. Heat Mass Transf.* **2018**, *126*, 531–543. [CrossRef]
32. Tiedemann, W.; Newman, J. Mathematical modeling of the lead-acid cell. In *Proceedings of the Symposium on Battery Design and Optimization*; The Electrochemical Society: Princeton, NJ, USA, 1979; pp. 1–79.
33. Lee, K.-J.; Smith, K.; Pesaran, A.; Kim, G.-H. Three dimensional thermal-, electrical-, and electrochemical-coupled model for cylindrical wound large format lithium-ion batteries. *J. Power Sources* **2013**, *241*, 20–32. [CrossRef]
34. Chen, M.; Rincon-Mora, G.A. Accurate electrical battery model capable of predicting runtime and IV performance. *IEEE Trans. energy Convers.* **2006**, *21*, 504–511. [CrossRef]
35. Pinto, A.M.; Oliveira, V.S.; Falcão, D.S.C. *Direct Alcohol Fuel Cells for Portable Applications: Fundamentals, Engineering and Advances*; Academic Press: Cambridge, MA, USA, 2018.
36. Barbir, F. *Pem Fuel Cells: Theory and Practice*; Academic Press: Cambridge, MA, USA, 2012.
37. Sucec, J. *Heat Transfer*; Jaico Publishing House: Mumbai, India, 1999.
38. Fan, Y.; Bao, Y.; Ling, C.; Chu, Y.; Tan, X.; Yang, S. Experimental study on the thermal management performance of air cooling for high energy density cylindrical lithium-ion batteries. *Appl. Therm. Eng.* **2019**, *155*, 96–109. [CrossRef]